AD_____

Award Number: W81XWH-10-1-0079

TITLE: Structure-Guided Insights into the Function of Merlin in Neurofibromatosis 2 (NF2)

PRINCIPAL INVESTIGATOR: Dr. Sollepura Yogesha

CONTRACTING ORGANIZATION: The Scripps Research Institute
La Jolla, CA 92037

REPORT DATE: August 2011

TYPE OF REPORT: Annual Summary

PREPARED FOR: U.S. Army Medical Research and Materiel Command
Fort Detrick, Maryland 21702-5012

REPORT DOCUMENTATION PAGE

Form Approved
OMB No. 0704-0188

1. REPORT DATE *(DD-MM-YYYY)*	2. REPORT TYPE	3. DATES COVERED *(From - To)*
01-08-2011	Annual Summary	15 Jan 2010 - 26 Aug 2011

4. TITLE AND SUBTITLE
Structure-Guided Insights into the Function of Merlin in Neurofibromatosis 2 (NF2)

5a. CONTRACT NUMBER

5b. GRANT NUMBER
W81XWH-10-1-0079

5c. PROGRAM ELEMENT NUMBER

6. AUTHOR(S)
Dr. Sollepura Yogesha

E-Mail: yogesha@scripps.edu

5d. PROJECT NUMBER

5e. TASK NUMBER

5f. WORK UNIT NUMBER

7. PERFORMING ORGANIZATION NAME(S) AND ADDRESS(ES)
The Scripps Research Institute
La Jolla, CA 92037

8. PERFORMING ORGANIZATION REPORT NUMBER

9. SPONSORING / MONITORING AGENCY NAME(S) AND ADDRESS(ES)
U.S. Army Medical Research and Materiel Command
Fort Detrick, Maryland 21702-5012

10. SPONSOR/MONITOR'S ACRONYM(S)

11. SPONSOR/MONITOR'S REPORT NUMBER(S)

12. DISTRIBUTION / AVAILABILITY STATEMENT
Approved for Public Release; Distribution Unlimited

13. SUPPLEMENTARY NOTES

14. ABSTRACT

Neurofibromatosis type 2 (NF2) is caused by inherited or sporadic mutations in the NF2 gene, and NF2 patients are highly prone to developing bilateral vestibular schwannomas or meningiomas. NF2 encodes two alternatively spliced forms, merlin-1 and merlin-2, which differ at their C-termini. Merlin belongs to ERM (ezrin-radixin-moesin) family of proteins that localize to adhesion complexes, bind to cell surface receptors and the actin cytoskeleton and, accordingly, play important roles in organizing cortical membrane domains. Finally the functions of ERM family proteins are regulated by alterations in their conformation triggered by binding to their partners, phosphorylation by select kinases, and by binding of acidic phospholipids. Although merlin shares sequence and structural similarity with ERM proteins, and merlin is unique in its capacity to function as tumor suppressor. We propose structural characterization of merlin by X-ray crystallography to determine the structure of merlin, its domains, and in complex with its interacting partners. By solving crystal structure of the human merlin-1 head:tail complex we provide important insight in to function of merlin. These studies explain the long-standing paradox of how the ostensibly 'closed' conformation of merlin-1 represents its tumor suppressor-active state. Complete understanding of the function would be possible from solving the structure of full length merlin and complex of merlin with other proteins which is in progress.

15. SUBJECT TERMS
Neurofibromatosis type 2 (NF2), FERM, crystal structure

16. SECURITY CLASSIFICATION OF:			17. LIMITATION OF ABSTRACT	18. NUMBER OF PAGES	19a. NAME OF RESPONSIBLE PERSON
a. REPORT	b. ABSTRACT	c. THIS PAGE			USAMRMC
U	U	U	UU	27	19b. TELEPHONE NUMBER *(include area code)*

Table of Contents

INTRODUCTION:

Neurofibromatosis type 2 (NF2) is caused by inherited or sporadic mutations in the *NF2* gene, and *NF2* patients are highly prone to developing bilateral vestibular schwannomas or meningiomas. *NF2* encodes two alternatively spliced forms, merlin-1 and merlin-2, which differ at their *C*-termini. Merlin belongs to ERM (ezrin-radixin-moesin) family of proteins that localize to adhesion complexes, bind to cell surface receptors and the actin cytoskeleton and, accordingly, play important roles in organizing cortical membrane domains. Finally the functions of ERM family proteins are regulated by alterations in their conformation triggered by binding to their partners, phosphorylation by select kinases, and by binding of acidic phospholipids (Figure 1).

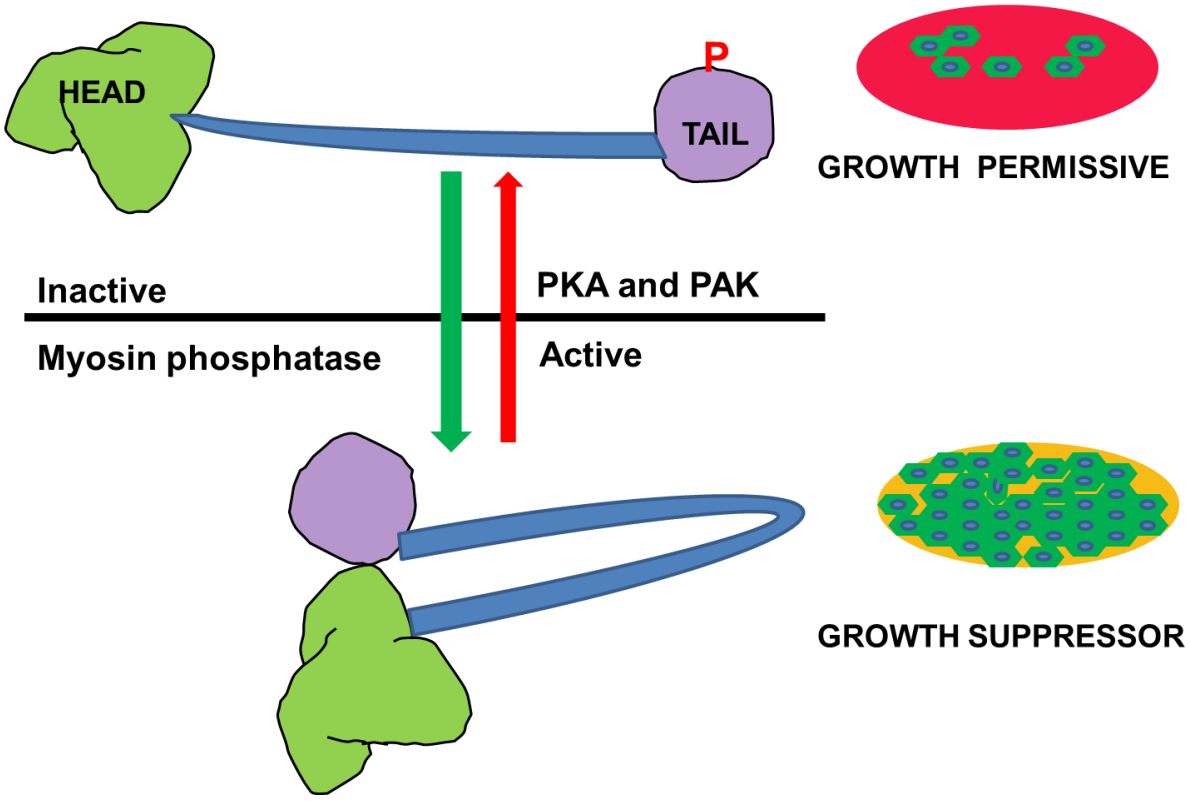

Figure 1. The tumor suppressor functions of merlin are controlled by phosphorylation (via PKA or PAK) and dephosphorylation (by myosin phosphatase). Phosphorylation is thought to disrupt merlin head-tail interactions that are necessary for it growth suppressive functions.

Given sequence similarities, as well as the crystal structures of the isolated FERM domain of merlin-1 (*1*) and those of the head:tail complex of ezrin (*2-4*) and that of full-length moesin (*5*) it was thought that the structure of native merlin-1 would be very similar to that of other ERM proteins, which are in a closed-clamp conformation that is directed by intramolecular interactions of the head (which contains the FERM domain) and tail domains. Thus, a major goal of our studies was to test this notion, by solving the crystal structure of the merlin-1 head:tail complex, as well of those of full-length merlin-1. Furthermore, it was known that merlin-1 could form

heterotypic, head-tail directed, interactions with other ERM family members in cells, specifically with ezrin and moesin (*6*), and that enforced expression of ezrin could impair the tumor suppressor functions of merlin-1. Furthermore, it has been suggested that the binding of Mediator-28 (Med28) can impair the tumor suppressor functions of the second merlin isoform, merlin-2. Thus, a second goal of our studies was to define the molecular underpinnings of these heterotypic interactions of merlin-1 and merlin-2.

BODY OF RESEARCH PROJECT:

The long-term goal of these fellowship studies was to define molecular mechanisms of the tumor suppression function of merlin by solving the structure of full-length merlin, the merlin head:tail complex, and the structures of merlin-1 in complex with its binding partners ezrin and Med28.

Aim 1. Crystal structure determination of merlin-1 head:tail complex and of full-length merlin-1
   a. Solve the crystal structure of merlin-1 head:tail complex
   b. Improve the merlin full length crystals

Aim 2. Crystal structure determination of the merlin-1:ezrin and merlin-2:med28 complexes.
   a. Solving crystal structure of ezrin head and merlin-1 tail complex
   b. Solving crystal structure of Med28 and merlin-2

Regarding our proposed studies of Aim 1, we solved the crystal structure of the merlin-1 head:tail complex. This structure is described in detail in our recently published article in *Protein Science*, and it revealed important insights regarding the intra-molecular interactions of the head and tail domains of merlin-1. First, although the FERM domain of tail-bound merlin-1 have an overall architecture akin to that of other ERM family proteins, with three subdomains F1, F2, and F3, surprisingly we found that binding of the tail provokes unfurling of the F2 subdomain of merlin as well as rotation of α-helix α3 away from the remainder of this subdomain – none of these features are present in the crystal structure of the head domain of merlin-1 alone (*1*, *7*); thus they are all provoked by binding of the tail of merlin-1. Specifically, α3 helix no longer interacts with the remainder of F2 subdomain but rather with the α1 α-helix of the F3 subdomain. Furthermore, there is also movement in the β6-β7 loop of the F3 subdomain. Finally, the tail was unstructured in this complex indicating that binding to the head domain also unfurls the tail domain. Collectively, these findings underscore the unique structure of the head:tail complex of merlin-1 versus those of other ERM family proteins, and they indicate that unlike other ERM family proteins merlin-1 head-tail interactions expose several new motifs in the protein that would allow them to interact with unique binding partners. A summary of the novel changes in the FERM domain structure provoked by bindings of the tail is provided in Figure 2.

To prove the relevance of the unique interactions revealed by the structure of the merlin-1 head:tail complex several domain swap (using motifs from the FERM domains of ezrin, moesin, and talin) mutants in the unfurled regions of F2 and the β6-β7 loop of merlin-1 were generated (Figure 3). These domain swap mutants were then cloned into lentiviral expression vectors that also express GFP so we can evaluate their biological effects in transduced primary wild type and *Nf2*$^{-/-}$ mouse Schwann cells that were kindly provided by our collaborator Dr. Marco Giovannini

(House and Ear institute, CA). A thorough analysis of the biological effects of these mutants will be the subject of future investigations.

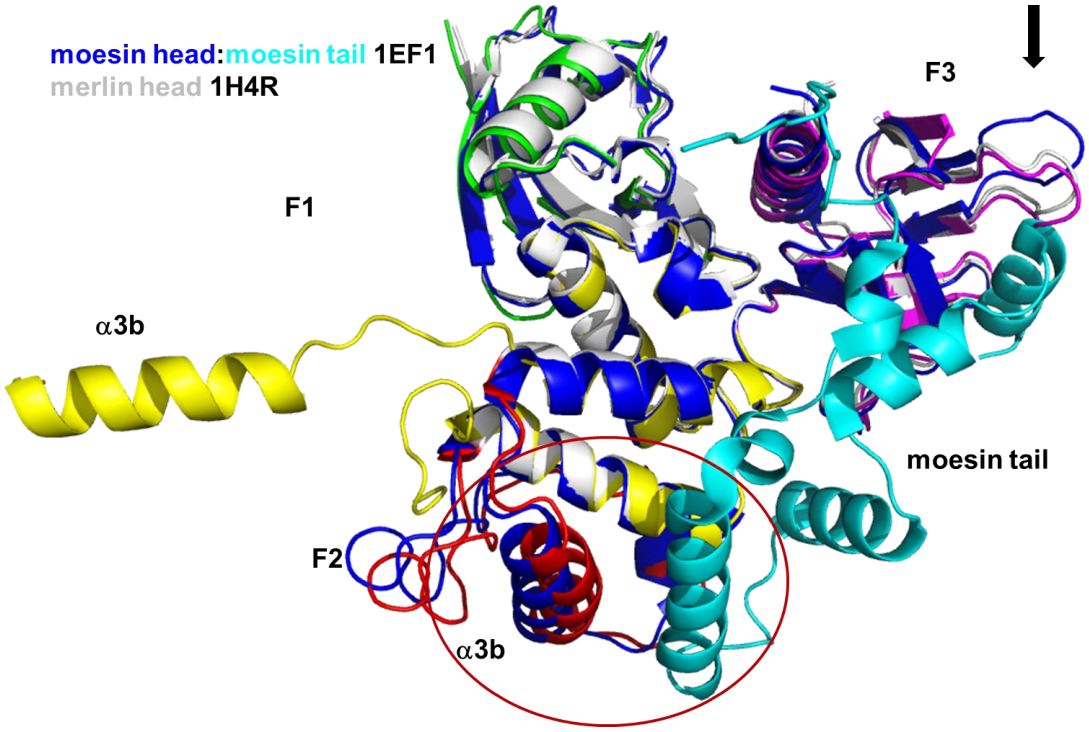

Figure 2. Superposition of our tail-bound merlin FERM domain structure onto the moesin FERM domain structure (PDB entry 1ef1) and human merlin FERM domain alone (PDB entry 1H4R). The F1 subdomain is shown in yellow, F2 in cyan and F3 in pink for the merlin FERM domain, and moesin structure is shown in blue/cyan. α3b and β6-β7 loops are labeled along with some secondary structure elements in F2 and F3 subdomains. The structure of the human FERM domain of merlin alone is shown in grey.

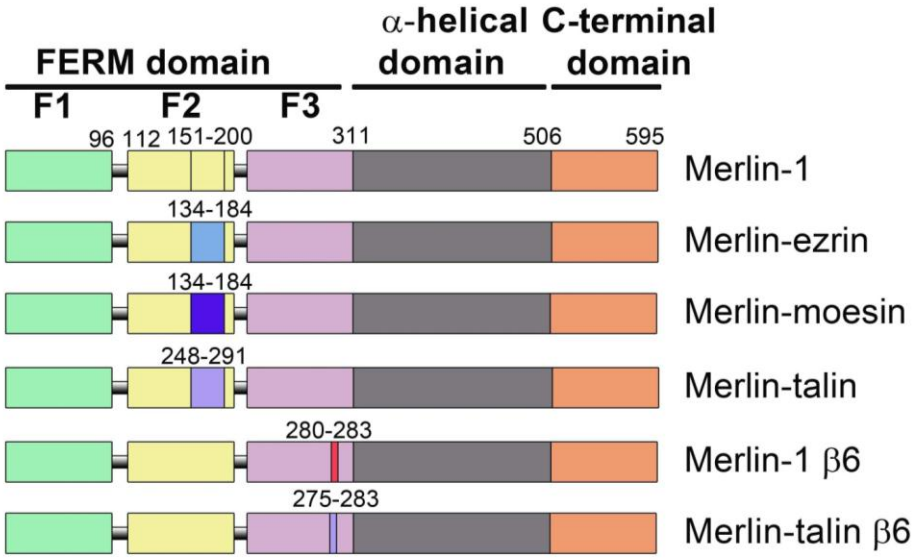

Fig 3. Summary of domain swap mutants generated in full-length merlin-1 to validate our structural findings.

We also generated GFP fusion constructs of wild type and mutant merlin-1. These constructs were transfected to HEK-293T cells to assess the effects of these mutations on the localization of merlin-1, which normally localizes to cell membranes, though a fraction of merlin-1 can also be detected in the nucleus. Notably, the subcellular localization of our domain swap merlin-1 mutants was similar to that of wild type merlin-1 (Figure 4).

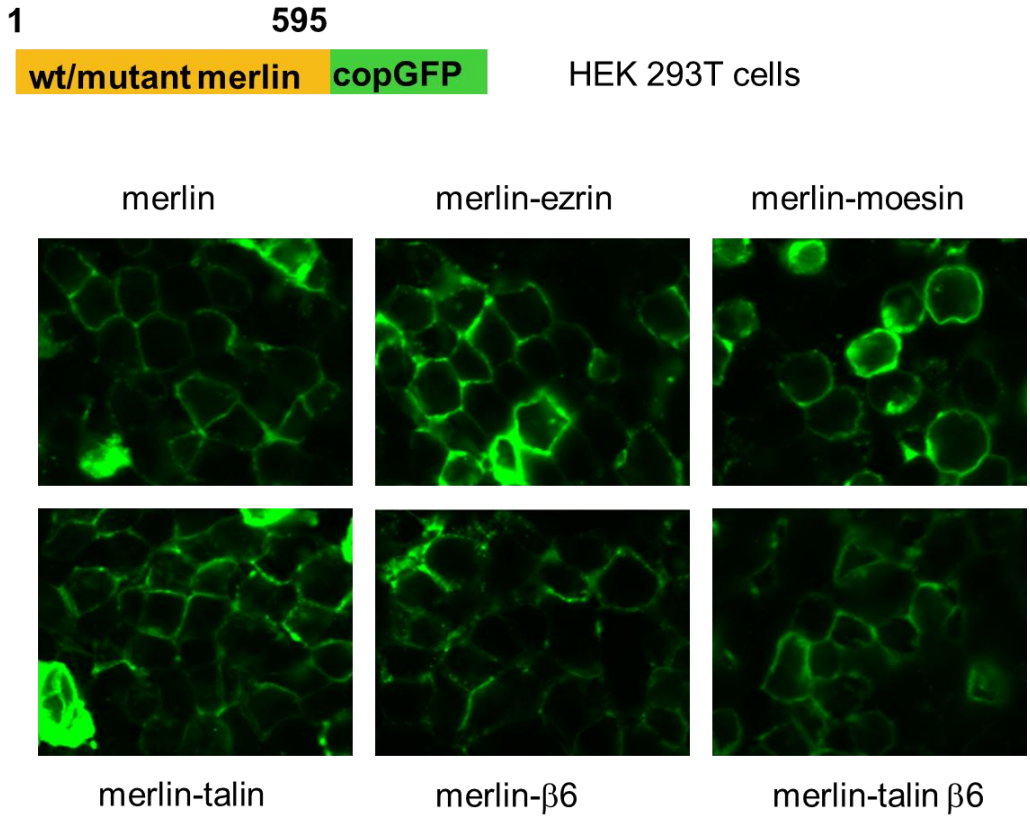

Fig 4. HEK-293T cells were transfected with the indicated GFP fusions of wild type and mutant forms of merlin-1 shown in Figure 3. As is evident, the localization of these domain swap mutants of merlin-1 is similar to that of GFP fusion of wild type merlin-1.

Regarding our the proposed studies of Aim 1b, to improve our crystals of full-length merlin, we received maltose-binding protein (MBP)fusion expression vectors from the laboratory of Dr. Lars Pederson (NIEHS-NIH, Research Triangle Park, North Carolina) that harbor entropy mutations on the surface of MBP, and which have been successfully used to yield crystals for several MBP fusion proteins that are difficult to crystallize. Full-length merlin-1 was cloned into these vectors and their sequences were confirmed. These constructs were checked for the expression of MBP-merlin-1 fusion proteins using BL21 (DE3) RIL bacteria and were shown to express levels of MBP-merlin-1 that were similar to our other merlin-1 expression constructs.

For the proposed studies of Aim 2a, we generated a new expression construct for the ezrin FERM domain, by fusing it in frame to an *N*-terminal cleavable His_8-tag that can be removed by precision protease. Following co-purification with the merlin-1 tail domain using a chelating nickel affinity chromatography column, the ezrin-head:merlin-1-tail complex was then treated with precision protease overnight at 4 ºC to remove the His_8-tag. The purified ezrin:merlin-1 complex without the tag was then purified using a Superdex-75 sizing chromatography column and this complex is being used in crystallization trials in the Izard laboratory.

Regarding the studies of Aim 2b, we successfully co-purified the merlin-2-tail:Med28 complex. Crystallization trials at both 4 ºC and ambient temperature have not yet yielded hits, but these screens will continue in the Izard laboratory.

KEY RESEARCH ACCOMPLISHMENTS: Key research accomplishments emanating from this research are as follows.

- Our merlin-1 tail-bound crystal structure of the merlin head domain suggests that the merlin-1 tail domain is highly dynamic in nature, as electron density for the tail is not found in the structure, despite the fact that the tail is bound to the head as judged by SDS-PAGE and mass spectrometry analyses.

- Binding of the merlin-1 tail domain provokes surprising movements and unfurling in the F2 motif of the merlin FERM domain.

- Movements in the F2 motif in the merlin-1 tail-bound structure of the head domain appear to direct dimerization of the merlin FERM domain. Given these findings we predict that dimerization of merlin-1 is essential for its functions as a tumor suppressor.

- The F2 domain is essential for the tumor suppressor functions of merlin (*8*). Thus, our findings suggest that F2 motif unfurling provoked by intramolecular interactions with the merlin-1 tail domain contribute to merlin-1 tumor suppressor functions.

- Movement of the loop in the F3 motif of the FERM domain is also predicted to contribute to merlin-1 tumor suppressor functions.

REPORTABLE OUTCOMES:

1. Abstract presented at American Crystallographic Association Meeting (ACA 2011) in New Orleans, LA, May 28- June 2, 2011 (copied below).

Unfurling of the F2 FERM domain of merlin tumor suppressor

S.D. Yogesha[1], Andrew J. Sharff[2], Marco Giovannini[3], Gerard Bricogne[2], and Tina Izard[1]

Cell Adhesion Laboratory, Department of Cancer Biology[1], The Scripps Research Institute, Florida 33458, USA; Global Phasing Ltd.[2], Sheraton House, Castle Park, Cambridge CB3 0AX, United Kingdom; and House Ear Institute[3], Center for Neural Tumor Research, Los Angeles, CA 90057, USA

Merlin is a tumor suppressor encoded by the *Neurofibromatosis-2* (*NF2*) gene and inactivation of *NF2* through mutations leads to development of nervous system tumors. Merlin is an ERM (ezrin, radixin, moesin) family cytoskeletal protein that interacts with other ERMs and with components of cell-cell adherens junctions (AJs), stabilizing these complexes. Loss of merlin destabilizes AJs, promoting cell migration and invasion, which in *Nf2*+/- mice leads to highly metastatic tumors. Merlin shares sequence and structural similarity with ERM proteins, and its capacity to bind F-actin and plasma membrane. But it is unique in its ability to suppress cell proliferation and ligand-induced cell signaling in many cell types, and to function as tumor suppressor. Paradoxically, the 'closed' conformation of merlin-1, where its *N*-terminal four-point-one/ezrin/radixin/moesin (FERM) domain binds to its *C*-terminal tail, directs its tumor suppressor functions. In this work, we report the crystal structure of the human merlin-1 head domain when crystallized in the presence of its tail domain. Remarkably, unlike other ERM head-tail interactions, this structure suggests that binding of the tail promotes dynamic movement and unfurling of the F2 motif of the FERM domain. Our 'open' structure of merlin-1 suggests that this unfurling of F2 domain directs dimerization of merlin-1 and may control its interaction with other proteins required for tumor suppression. We conclude that the 'closed' tumor suppressor conformation of merlin-1 is in fact an 'open' dimer whose functions are disabled by *NF2* mutations that disrupt this architecture.

2. All of our structural findings were published in *Protein Science* in our article entitled "*Unfurling of the band 4.1, ezrin, radixin, moesin (FERM) domain of the merlin tumor suppressor*" (pdf attached).

CONCLUSIONS:

Our DOD-supported studies solved the first structure of the merlin-1 head domain in complex with its tail, and these findings have provided important new insights into our understanding of the functions of this unique tumor suppressor. In particular, our studies indicate that the intramolecular interactions of head and tail domains that hold other ERM family proteins in a closed-clamp conformation actually direct a highly dynamic open structure for merlin-1. These studies explain the long-standing paradox of how the ostensibly 'closed' conformation of merlin-1 represents its tumor suppressor-active state. That is, merlin-1 in its native state is highly dynamic, where motifs in both the head and tail domain are unfurled and represent possible docking sites for binding partners that contribute to the tumor suppressor functions of merlin. These studies provide a critical foundation for the campaigns of the Izard laboratory to solve the crystal structure of full-length merlin-1, as well as those of merlin-1 in complex with ezrin and other ERM family members. They also will help resolve how the tumor suppressor functions of merlin-1 are abolished via heterotypic interactions with ezrin or moesin. Finally, these studies also form a foundation for the development of new small molecules that specifically disrupt the unique interactions of the tail and head of merlin, which may well prove efficacious in the treatment of *NF2* patients bearing Schwannomas or meningiomas

REFERENCES:

1. B. S. Kang, D. R. Cooper, Y. Devedjiev, U. Derewenda, Z. S. Derewenda, The structure of the FERM domain of merlin, the neurofibromatosis type 2 gene product. *Acta Crystallogr D Biol Crystallogr* **58**, 381 (Mar, 2002).
2. W. J. Smith, N. Nassar, A. Bretscher, R. A. Cerione, P. A. Karplus, Structure of the active N-terminal domain of Ezrin. Conformational and mobility changes identify keystone interactions. *J Biol Chem* **278**, 4949 (Feb 14, 2003).
3. S. D. Edwards, N. H. Keep, The 2.7 A crystal structure of the activated FERM domain of moesin: an analysis of structural changes on activation. *Biochemistry* **40**, 7061 (Jun 19, 2001).
4. M. A. Pearson, D. Reczek, A. Bretscher, P. A. Karplus, Structure of the ERM protein moesin reveals the FERM domain fold masked by an extended actin binding tail domain. *Cell* **101**, 259 (Apr 28, 2000).
5. Q. Li *et al.*, Self-masking in an intact ERM-merlin protein: an active role for the central alpha-helical domain. *J Mol Biol* **365**, 1446 (Feb 2, 2007).
6. R. Nguyen, D. Reczek, A. Bretscher, Hierarchy of merlin and ezrin N- and C-terminal domain interactions in homo- and heterotypic associations and their relationship to binding of scaffolding proteins EBP50 and E3KARP. *J Biol Chem* **276**, 7621 (Mar 9, 2001).
7. T. Shimizu *et al.*, Structural basis for neurofibromatosis type 2. Crystal structure of the merlin FERM domain. *J Biol Chem* **277**, 10332 (Mar 22, 2002).
8. D. Lallemand, A. L. Saint-Amaux, M. Giovannini, Tumor-suppression functions of merlin are independent of its role as an organizer of the actin cytoskeleton in Schwann cells. *J Cell Sci* **122**, 4141 (Nov 15, 2009).

APPENDICES:

Protein Science article has been attached

SUPPORTING DATA: None

PROTEIN STRUCTURE REPORT

Unfurling of the band 4.1, ezrin, radixin, moesin (FERM) domain of the merlin tumor suppressor

S. D. Yogesha,[1] Andrew J. Sharff,[2] Marco Giovannini,[3] Gerard Bricogne,[2] and Tina Izard[1]*

[1]Cell Adhesion Laboratory, Department of Cancer Biology, The Scripps Research Institute, Jupiter, Florida 33458
[2]Global Phasing Ltd., Sheraton House, Castle Park, Cambridge CB3 0AX, United Kingdom
[3]House Ear Institute, Center for Neural Tumor Research, Los Angeles, California 90057

Received 3 August 2011; Accepted 7 October 2011
DOI: 10.1002/pro.751
Published online 19 October 2011 proteinscience.org

Abstract: The merlin-1 tumor suppressor is encoded by the Neurofibromatosis-2 (Nf2) gene and loss-of-function Nf2 mutations lead to nervous system tumors in man and to several tumor types in mice. Merlin is an ERM (ezrin, radixin, moesin) family cytoskeletal protein that interacts with other ERM proteins and with components of cell–cell adherens junctions (AJs). Merlin stabilizes the links of AJs to the actin cytoskeleton. Thus, its loss destabilizes AJs, promoting cell migration and invasion, which in $Nf2^{+/-}$ mice leads to highly metastatic tumors. Paradoxically, the "closed" conformation of merlin-1, where its N-terminal four-point-one, ezrin, radixin, moesin (FERM) domain binds to its C-terminal tail domain, directs its tumor suppressor functions. Here we report the crystal structure of the human merlin-1 head domain when crystallized in the presence of its tail domain. Remarkably, unlike other ERM head–tail interactions, this structure suggests that binding of the tail provokes dimerization and dynamic movement and unfurling of the F2 motif of the FERM domain. We conclude the "closed" tumor suppressor conformer of merlin-1 is in fact an "open" dimer whose functions are disabled by Nf2 mutations that disrupt this architecture.

Keywords: actin cytoskeleton; adherens junctions; crystallography; neurofibromatosis

Introduction

Loss-of-function, generally nonsense point mutations in merlin manifest in familial *Nf2* lead to rare bilateral vestibular schwannoma and meningioma,[1] whereas biallelic inactivation of *Nf2* occurs in sporadic schwannoma,[2] meningiomas,[3] and malignant mesothelioma.[4] Furthermore, merlin proteins probably play broad roles in suppressing cancer, as heterozygous $Nf2^{+/-}$ mice, which express only half the level of these scaffold proteins in their tissues, are prone to developing a wide array of aggressive

Abbreviations: AJ, adherens junctions; CCP4, collaborative computational project Nr.4; ERM, ezrin, radixin, moesin; FERM, four-point-one ERM; *Nf2*, neurofibromatosis-2; NHERF, Na^+-H^+ exchanger regulatory factor; PEG, polyethylene glycol; PIP_2, phosphatidylinositol 4,5-bisphosphate.

Additional Supporting Information may be found in the online version of this article.

Grant sponsors: National Institutes of Health; State of Florida.

*Correspondence to: Tina Izard, Cell Adhesion Laboratory, Department of Cancer Biology, The Scripps Research Institute, Jupiter, FL 33458. E-mail: mkernick@scripps.edu

tumors, including sarcoma and carcinoma.[5,6] Merlin-1 and merlin-2 are unique amongst tumor suppressors in that they localize to and somehow stabilize maturing adherens junction (AJ) complexes that mediate cell–cell contacts[7] and that are directed by homotypic interactions of cadherin receptors. Further, merlin proteins also suppress the cell surface expression of transmembrane growth factor receptors.[8,9] Finally, they also associate with the actin network, either directly via interactions of their *N*-termini with actin,[10–12] or indirectly via heterotypic interactions with other ezrin, radixin, moesin (ERM) family members.[13] Importantly, these functions are necessary for proper development, cell growth, and contact inhibition, and for harnessing tumorigenesis.

ERM proteins provide essential links of AJs to the actin cytoskeleton,[14] play important roles in remodeling AJs during epithelial morphogenesis, and maintain organized apical surfaces on the plasma membrane.[10] ERM proteins belong to the band 4.1 superfamily that shares an ~300-residue globular FERM domain comprised of three subdomains (F1, F2, and F3), whose structure resembles that of a cloverleaf.[15] These proteins also harbor a central α-helical rod domain and a *C*-terminal domain that directs F-actin interactions. The overall architecture of merlin is thought to be similar to that of ERM proteins, as they have a FERM domain and a central α-helical rod, but lack a *C*-terminal actin-binding site.

All ERM proteins appear to be regulated by transitioning from a closed conformation to an open, active state following severing of intramolecular head–tail interactions, and of interactions between their head and central α-helical domains. The crystal structures of the FERM domains of ezrin and merlin,[16–18] the moesin head:tail complex, and the moesin FERM domain in complex with its central α-helical domain have been solved.[15,19] The moesin head:tail complex structure established that this interaction buries the charged F-actin binding site, and that the *C*-terminal tail covers large portions of the F2 and F3 motifs of the FERM domain. Conformational changes that occur when these proteins switch to their activated state are thought to sever these intramolecular contacts, allowing these proteins to open and bind to their other partners.

How ERM proteins are activated is not entirely resolved, but this is a Rho dependent process[20] and is triggered by binding to other protein ligands or phospholipids or by phosphorylation as seen with merlin-1.[21] For example, the binding of the FERM domain of ERM proteins to the cytoplasmic tails of ICAMs or the adaptor protein EBP50 displaces the ERM *C*-terminal tail despite their binding sites not overlapping.[22,23] Further, the binding of a basic cleft that lies between the F1 and F3 subdomains to phosphatidylinositol 4,5-bisphosphate (PIP_2) directs ERM proteins to the plasma membrane, and may also sever their head–tail interactions.[24] Finally, phosphorylation of conserved threonine residues in the ERM *C*-terminal actin-binding site is necessary for their localization to AJs and for binding to the actin cytoskeleton, and maintains ERM proteins in their active state. Probably all three triggers, phosphorylation and binding to PIP_2 and protein partners, is necessary for full activation of ERM proteins.[25]

What triggers sever the supposedly "closed," tumor suppressor-active form of merlin-1 is less clear, although Ser-10 and Ser-518 phosphorylation by PKA and/or PAK have been proposed to have a role in this response.[26,27] Further, phosphomimetic mutants of these sites impair merlin-1 tumor suppression functions and these mutants directly interact with other partners in cells, such as ezrin.[28] Binding partners for ERM proteins include each other, and selected adhesion proteins and adapters that direct association with membrane-spanning proteins. For example, the *C*-terminal domains of the EBP50 and E3KARP members of the NHERF (Na^+-H^+ Exchanger Regulatory Factor) family bind to ezrin and merlin, and link ERMs to membrane proteins such as NHE3 and CTFR through the agency of their PDZ domains.[29] In addition, ERM proteins and merlin also directly bind to adhesion receptors, including NHERF,[30] CD44,[31] and E-cadherin.[7]

To define the ostensibly closed, tumor suppressor-active state of merlin-1, we crystallized the human merlin-1 head:tail complex. While no electron density is visible for the tail domain in this structure the F2 domain is unfurled, suggesting that binding of the merlin-1 tail promotes movement and unfurling of its F2 motif. Thus, merlin is actually in an "open" conformation relative to other ERM members, perhaps explaining its tumor suppressor function.

Results

Overall crystal structure

We copurified the merlin-1 head and tail domains and crystallized the head:tail complex. SDS-PAGE (SDY, unpublished data) and mass spectrometry analyses confirmed the presence of the tail domain in these crystals (Supporting Information Table). However, electron density was only observed for the head domain. The final model is comprised of residues 20–82, 91–152, 178–312 (chain "A"); 20–82, 91–152, 178–312 ("B"); 20–82, 91–158, 178–312 ("C"); and 20–82, 91–150, and 199–312 ("D"). As seen in other isolated FERM domain structures, and in the moesin head:tail structure,[15] the structure of the merlin head domains harbors three subdomains (F1, F2, and F3) [Fig. 1(A)] having fold similarities to known single-domain proteins.[32] The F1 subdomain resembles ubiquitin, whereas F2 shares structural

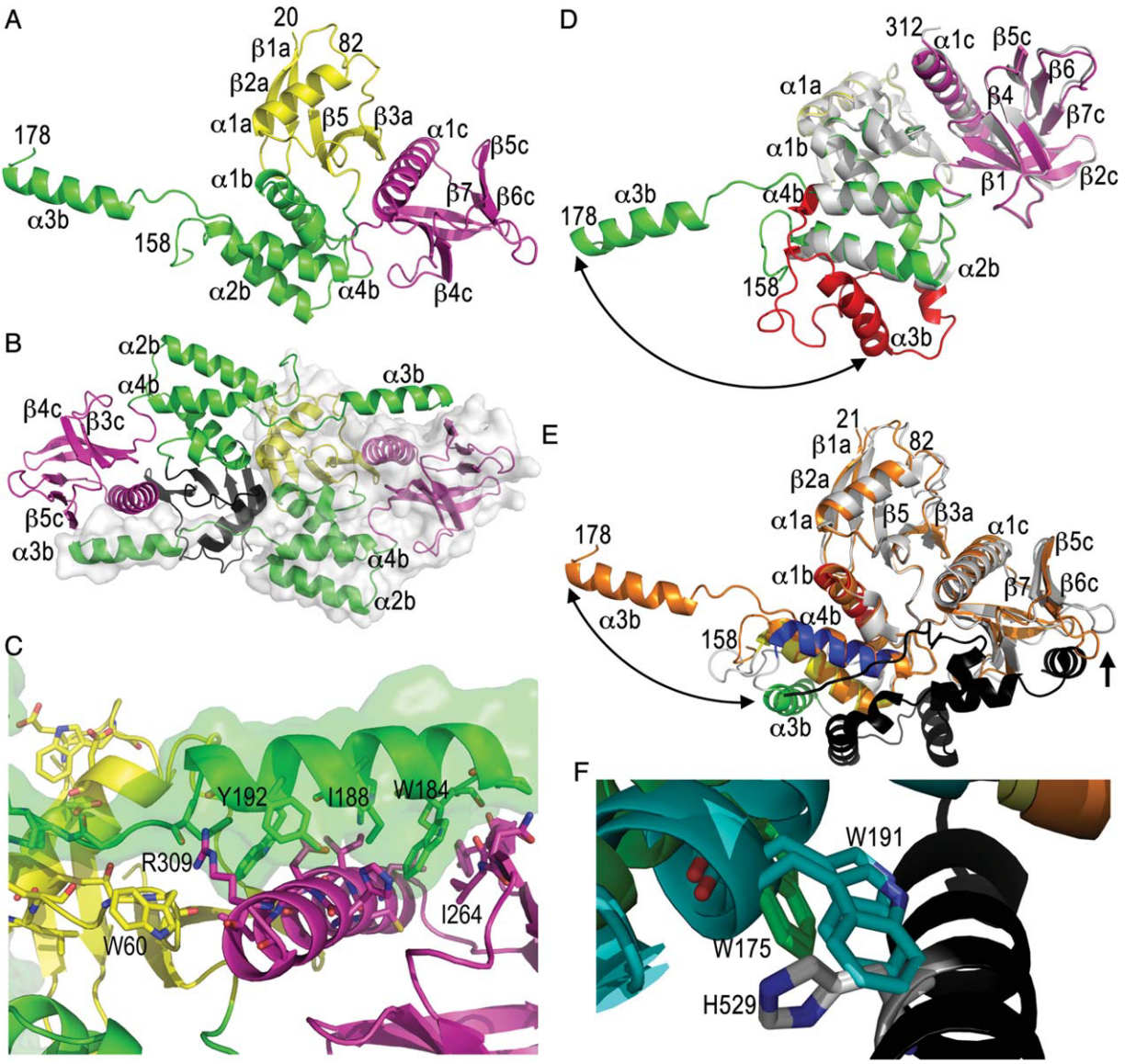

Figure 1. The merlin FERM domain structure is unfurled. (A) Cartoon drawing of the human merlin head FERM domain. The F1 subdomain (residues 20–82 and 91–100) is shown in yellow, the F2 subdomain (residues 101–158 and 178–215) is shown in green, and the F3 motif (residues 216–313) is shown in magenta. Some termini (21, 82, 158, and 178) and secondary structure elements ("a" belonging to the F1, "b" to F2, and "c" to the F3 subdomains) are labeled in several panels. (B) The unfurled F2 subdomain engages in additional contacts with another monomer, which is shown as a surface representation. The FERM subdomains are colored as in panel (A) (F1, yellow or black; F2, green; and F3, magenta). (C) Detailed view of the intermolecular interactions of the extended F2 α3b α-helix (F2, green) with a two-fold related molecule (F1, yellow; and F3, magenta). A surface representation is also shown for the F2 subdomain. (D) Superposition of our unfurled merlin head domain (molecule "C"; F1, yellow; F2, green; and F3, magenta) onto the closed, unbound FERM domain structure of merlin (PDB entry 1h4r; white and red) is shown. The two molecules in the closed FERM structure superimpose with r.m.s.d. of 1.3 and 1.4 Å for 1965 atoms of our unfurled merlin structure. The large movement of the α-helix α3b of the F2 subdomain (red) is indicated by the arrow. (E) Superposition of the unfurled merlin structure (molecule "C," orange) onto the moesin head:tail complex structure (PDB entry 1ef1; F1 and F2, white; F2 α-helix α1b, moesin residues 95–112, red; F2 α2b α-helix, moesin residues 118–135, yellow; F2 α3b α-helix, moesin residues 164–179, green; F2 α-helix α4b, moesin residues 183–196, blue; tail, black) with r.m.s.d. of 1.9 Å for 1780 atoms of the two moesin FERM domains in the asymmetric unit. The large movement of α-helix α3b is indicated by a double arrow. The movement of the β6c-β7c loop that seems necessary to allow tail binding is indicated by an arrow. (F) Close-up view of the movement of the α-helix α3b upon tail binding. Trp191 residing on the F2 α-helix α3b of the superimposed closed, unbound merlin FERM conformation clashes with the tail domain, in particular with His529.

similarities with the acyl-CoA binding protein, and F3 has structural homology to phosphotyrosine binding (PTB), pleckstrin homology (PH), and Enabled/VASP Homology 1 (EVH1) signaling domains. In particular, in all reported structures, the F2 FERM subdomain is comprised of four α-helices that form a compact bowl-like structure. To our surprise, the F2 subdomain of the merlin FERM domain is unfurled and the F2 α3b α-helix is rotated away from the remainder of this subdomain. The unfurled F2 subdomain is seen in all four subunits in the symmetric unit and all four subunits are very similar. The F2 α3b α-helix (residues 151–201) does not interact with the remainder of this subdomain as seen in the native structure of the merlin head domain alone[17] but with the α-helix α1c of the F3 subdomain of a two-fold related molecule [Fig. 1(B); Supporting Information Fig. S1]. Further, the loop that follows the F2 α-helix α2b (residues 151–158) engages in hydrophobic interactions with the side chains of Lys44, Asp45, Asp48, and Arg52 of the α-helix α1a of the F1 subdomain, and there are also electrostatic interactions between Asp152 and Arg52. In addition, the extended F2 α-helix α3b and its preceding region (residues 178–192) engage in hydrophobic contacts with Asn263, Ile264, Ser265, Leu297, Cys300, Ile301, Gly302, Asp305, and Leu306, which are located on the β-strand β5c (262–267) and α-helix α1c (290–311) of the two-fold related F3 subdomain [Fig. 1(C)]. Hydrogen-bond interactions of Met179 with Tyr266, Ile188 with Asp305, and Tyr192 with Arg309 are also manifest. Finally, the new extended loop connecting F2 α-helices α3b and α4b (residues 194–202) engages in hydrophobic interactions not seen in other FERM structures with the side chains of Cys51, Arg52, Arg57, Thr59, and Trp60, which are located on the two-fold related F1 subdomain α-helix α1a and its following loop. Hydrogen bond interactions of His195 with Arg309 and Arg198 with Leu56, Arg57, and Thr59 are also found in this contact area.

Superposition of our unfurled merlin head domain structure onto the 1.8 Å structure of the merlin head domain alone[17] shows that the F1 and F3 subdomains, and the α-helices α1b, α2b, and α4b regions of F2, are almost identical with r.m.s.d. of less than 0.6 Å for 1,704 atoms of residues 20–147 and 202–312 [Fig. 1(D)]. Similar results are obtained in a superposition with the mouse merlin FERM domain crystal structure.[18] However, in our structure the last turn of the α2b α-helix of the F2 subdomain unfurls, thereby extending the following loop region and moving α-helix α3b to a completely new position, which also results in movement of the *N*-terminus of the F2 α-helix α4b.

Superposition with the 3 Å full-length moesin crystal structure[33] (Supporting Information Fig. S2A) shows that the *C*-terminal region of the additional α-helix A of the central domain in moesin and the A–B loop prevents unfurling of its FERM domain. However, the central α-helical region, harboring α-helices A and B, is divergent between merlin and moesin with only 30% sequence identity.

Superposition with the moesin head:tail complex crystal structure [Fig. 1(E)] shows additional novel features of the F3 β6c-β7c loop (merlin residues 275–283), where this loop in our unfurled merlin FERM domain is located further away from the tail domain-binding site present in moesin, presumably to allow binding of the merlin-1 tail. Further, superposition of the closed, merlin structure, the moesin head–tail structure, and our unfurled head domain established that the β6c-β7c loop displays the conformation seen in the moesin head:tail complex structure allowing tail binding (Supporting Information Fig. S2B). Importantly, the F2 α-helix α3b, in particular Trp191 residing on α3b, prevents tail domain binding in the unbound merlin structure [Fig. 1(F)]. Indeed, the F2 α-helix α3b is shifted in the moesin head:tail structure to allow binding of the tail domain. Moreover, crystal contacts are not compatible with the tail binding as seen for moesin. We conclude that binding of the tail domain induces movements in the FERM domain, which could be initiating events for further unfurling of this region in merlin. Interestingly, there is only 43% identity in regions of divergent conformation (merlin residues 150–201), yet there is 53 and 74% identity in the 51 residues before (merlin residues 98–149) or after (merlin residues 202–253) this unfurled region (Supporting Information Fig. S3).

Dimerization

Full-length merlin-1 is a monomer in high salt (500 m*M*) yet forms homodimers and higher-order oligomers under physiological conditions.[29] Further, two-hybrid interaction analyses[34] and *in vitro* binding assays[35] suggest that the merlin-1 homodimer is the active form of the protein.[36] In our unfurled merlin head structure the interface between molecules A and C (or B and D) in the asymmetric unit is highly significant, where over 5,500 Å^2 total solvent accessible surface area is buried, corresponding to almost 18% of the solvent accessible surface area. Moreover, the shape correlation statistic derived using the CCP4 program SC[37] is 0.726 for this interface, a significant value where a value of 1 indicates perfect fit versus 0.35 indicates the mismatch of an artificial association. Further, the shape correlation statistics for the α-helix α3b of the F2 subdomain correspond to 0.801. These values suggest that the crystallographic dyad represents a homodimer in solution. Unfortunately, the heterogeneity of the protein domains prevented dynamic and static light scattering (DLS and SLS) experiments to determine their oligomeric state in solution (SDY, unpublished data),

a difficulty that has also been encountered by others.[29]

Discussion

We crystallized the merlin head:tail complex but electron density is only observed for the head domain; thus, the tail domain of merlin-1 is probably highly dynamic. Importantly, the binding of the tail domain provokes surprising movements and unfurling in the F2 motif of the merlin FERM domain. Further, this unfurling in the merlin head domain directs extensive interactions with a two-fold related molecule. To our knowledge the unfurling of any motif of the FERM domain is unprecedented and indeed all FERM structures are very similar. Thus, merlin stands alone in its architecture of this domain, which we propose plays important roles in merlin tumor suppressor functions. In support of this notion, the F2 subdomain was recently shown to be essential for merlin to suppress the proliferation of primary *Nf2*-deficient Schwann cells.[38] The merlin F2 domain also harbors a submotif called the blue box (177-YQMTPEM-183), which is conserved in other species but not in ERM proteins.[39] In *Drosophila*, a blue box mutant acts as a dominant negative, underscoring the importance of this region in merlin functions. Precisely how this motif contributes to merlin function is, however, unclear, as the blue box is disordered in our structure.

The extensive dyad interactions that are manifest in our unfurled merlin head domain structure are also unique for FERM domains. Although a dimeric 2.8 Å radixin structure[40] showed that a domain swap of the *C*-terminal β-strand is involved in dimeric interactions, those present in the merlin structure are six-fold greater in their buried accessible surface area. Indeed, this interface in the merlin structure (2,800 Å^2 per polypeptide chain) lies well within those observed for established homodimers, which range from 370 to 4,750 Å.[2,41] While large crystal contacts have been observed for up to 900 Å^2, at least for monomeric lysozyme,[42] the merlin FERM-FERM interface is more than three times greater than that of the unusually large crystal–crystal contacts of lysozyme.

Effects of salt on the oligomerization of full-length merlin-1 have been reported,[29] where increases in salt concentration have been suggested to sever the head:tail interaction and impair the higher-order oligomers present under physiological conditions. Indeed, the previously determined unbound merlin head domain structure was monomeric and crystallized in 56% saturated ammonium sulfate.[17] By contrast, our dimeric merlin head:tail complex crystallization was performed with 20-fold less ammonium sulfate. We hypothesize that tail domain-induced unfurling of the F2 subdomain directs dimerization and that this response is manifest in full-length merlin-1.

The structure presented herein provides important clues as to how merlin functions as a tumor suppressor. The head:tail structures of ERM proteins and of full-length moesin[33] have revealed a tight globular closed architecture. By contrast, our unfurled merlin FERM structure shows that at least the F2 subdomain is in an "open" configuration, where it may direct merlin-1 dimerization and/or its interactions with partners required for tumor suppression. Thus, loss-of-function mutations found in the head and tail domains in *Nf2* may prevent the binding of these open domains to other partners and/or dimerization of merlin-1, which may also be required for its tumor suppressor functions.

Materials and Methods

Protein preparation

Human *merlin-1* complementary DNA corresponding to its head domain (residues 18–312) was amplified and cloned into pGEX-6P-1 expression vector (GE Life Sciences) using the *Bam*HI and *Xho*I restriction sites. The untagged merlin-1 tail domain (residues 503–595) was amplified and cloned into pET24b expression vector (Novagen) using the *Nde*I and *Xho*I restriction sites. Proteins were expressed in *Escherichia coli* BL21(DE3)RIL (Stratagene) at 25°C for 20 h in Luria–Bertani medium with ampicillin (GST-head) or kanamycin (tail). Cells were pooled and lysed in 50 m*M* Tris, 300 m*M* NaCl (pH 8), and complete mini protease inhibitor tablet (Roche) and ultracentrifuged at 95,834*g* for 1 h. Proteins were copurified using a GST FF chromatography affinity column (GE Life Sciences) and eluted with 10 m*M* reduced glutathione. The GST-tag was removed by incubating 1 U PreScission protease per mg of protein in 50 m*M* Tris 150 m*M* NaCl, 1 m*M* DTT, 1 m*M* EDTA, pH 7.5, for 24 h at 4°C. The head:tail complex was further purified using a Superdex 75 26/60 gel filtration chromatography column (GE Life Sciences) equilibrated with 50 m*M* Tris and 300 m*M* NaCl (pH 8). The purified complex was concentrated to 5.6 mg mL^{-1}.

Crystallization and X-ray data collection and reduction

Initial crystallization hits were identified using the Lite crystallization screen (Hampton Research) at 4°C. Two similar conditions, both containing 200 m*M* ammonium sulfate and polyethylene glycol (PEG), produced microcrystals. Best crystals were obtained from 4.5% PEG-4000 and 0.2 *M* ammonium sulfate.

X-ray diffraction data were collected at the Advanced Photon Source, SER-CAT beamline 22ID,

Table I. *X-Ray Data Reduction and Crystallographic Refinement Statistics*

(A) X-ray data reduction statistics	
Space group	$P422$
Unit cell parameters ($a = b$, c)	105.45 Å, 330 Å
Wavelength	0.99999 Å
Resolution (last shell)	26.36–2.64 Å (2.78–2.64 Å)
R-merge[a] (last shell)	0.063 (0.377)
Total no. of observations	376,916 (12,653)
Total no. of unique reflections	52,570 (6182)
Average $I/\sigma(I)$ (last shell)	19.9 (1.9)
Completeness (last shell)	0.952 (0.797)
Redundancy (last shell)	7.2 (2)

(B) Crystallographic refinement statistics	
Space group	$P4_12_12$
Unit cell parameters ($a = b$, c)	105.45 Å, 330 Å
Low (high) resolution limit	38.65–2.64 Å (2.71–2.64 Å)
No. of reflections, working set (last shell)	49,850 (2626)
No. of reflections, test set (last shell)	2666 (128)
R-factor[b] (last shell)	0.2003 (0.2340)
R-free[c] (last shell)	0.2294 (0.2703)
No. of residues	1023
No. of protein atoms	8540
No. of solvent atoms	537
Average B-factor (protein)	65.8 Å^2
Average B-factor (solvent)	54.8 Å^2
Overall anisotropy B11, B22, B33	0.61620 Å^2, 0.61620 Å^2, 1.23240 Å^2
R.m.s.d. from ideal values	
Bond length	0.008 Å
Bond angle	0.87°

[a] $R\text{-merge} = \sum_{hkl}\sum_{i}|I_i(hkl) - \overline{I(hkl)}|/.\sum_{hkl}\sum_{i}I_i(hkl)$.

[b] $R\text{-factor} = \sum_{hkl}||F_{obs}(hkl)|-|F_{calc}(hkl)||/.\sum_{hkl}|F_{obs}(hkl)|$, where $<|F_{calc}|>$ denotes the expectation of $|F_{calc}(hkl)|$ used in defining the likelihood refinement target.

[c] The free R-factor is a cross-validation residual calculated by using about 5% reflections, which were randomly chosen and excluded from the refinement.

at the Argonne National Laboratory and processed with autoProc[43] utilizing XDS[44] and SCALA.[45] The data were reduced in space group P422, as the pattern of systematic absences precluded unambiguous assignment of the space group at this stage (Table I).

Structure determination and crystallographic refinement

Phases were obtained by molecular replacement using the merlin-1 head domain structure as a search model and the program PHASER.[46] We searched in all appropriate space groups and obtained four solutions in $P4_12_12$ and confirmed the space group with the CCP4 program SFTOOLS.[47] Eight rounds of crystallographic refinement were performed with autoBUSTER[48] with manual inspection and model building with Coot.[49] The first round of refinement included a cycle of rigid body refinement. Automatic LSSR NCS restraints[50] were applied throughout and water was added in the sixth round of refinement using the "findwater" routine in Coot.[49] The final crystallographic refinement statistics are shown in Table I.

PDB Coordinates

The coordinates have been deposited with the Protein Data Bank (PDB entry 3u8z).

Acknowledgment

The authors are indebted to colleagues at Scripps FL: Philippe Bois for initiating the project and fruitful discussions, John Cleveland for discussions and critical review of the manuscript, Zhen Wu and Philippe Bois for sequencing, and HaJeung Park and Erumbi Rangarajan for substantial help with data collection. They thank Kristie Rose for mass spectrometry experiments and peptide analyses. Finally, they are grateful to the staff at the Advanced Photon Source, SER-CAT, for their synchrotron support. SDY is a fellow of the Department of Defense Neurofibromatosis Research Program. This is publication number 20731 from The Scripps Research Institute.

References

1. McClatchey AI, Giovannini M (2005) Membrane organization and tumorigenesis—the NF2 tumor suppressor, Merlin. Genes Dev 19:2265–2277.
2. Stemmer-Rachamimov AO, Xu L, Gonzalez-Agosti C, Burwick JA, Pinney D, Beauchamp R, Jacoby LB, Gusella JF, Ramesh V, Louis DN (1997) Universal absence of merlin, but not other ERM family members, in schwannomas. Am J Pathol 151:1649–1654.
3. Ruttledge MH, Sarrazin J, Rangaratnam S, Phelan CM, Twist E, Merel P, Delattre O, Thomas G, Nordenskjold M, Collins VP, Dumanski JP, Rouleau GA (1994) Evidence for the complete inactivation of the NF2 gene in the majority of sporadic meningiomas. Nat Genet 6:180–184.
4. Bianchi AB, Mitsunaga SI, Cheng JQ, Klein WM, Jhanwar SC, Seizinger B, Kley N, Klein-Szanto AJ, Testa JR (1995) High frequency of inactivating mutations in the neurofibromatosis type 2 gene (NF2) in primary malignant mesotheliomas. Proc Natl Acad Sci USA 92:10854–10858.
5. Giovannini M, Robanus-Maandag E, van der Valk M, Niwa-Kawakita M, Abramowski V, Goutebroze L, Woodruff JM, Berns A, Thomas G (2000) Conditional biallelic Nf2 mutation in the mouse promotes manifestations of human neurofibromatosis type 2. Genes Dev 14:1617–1630.
6. McClatchey AI, Saotome I, Mercer K, Crowley D, Gusella JF, Bronson RT, Jacks T (1998) Mice heterozygous for a mutation at the Nf2 tumor suppressor locus develop a range of highly metastatic tumors. Genes Dev 12:1121–1133.
7. Lallemand D, Curto M, Saotome I, Giovannini M, McClatchey AI (2003) NF2 deficiency promotes tumorigenesis and metastasis by destabilizing adherens junctions. Genes Dev 17:1090–1100.

8. Curto M, Cole BK, Lallemand D, Liu CH, McClatchey AI (2007) Contact-dependent inhibition of EGFR signaling by Nf2/Merlin. J Cell Biol 177:893–903.
9. Maitra S, Kulikauskas RM, Gavilan H, Fehon RG (2006) The tumor suppressors Merlin and expanded function cooperatively to modulate receptor endocytosis and signaling. Curr Biol 16:702–709.
10. Brault E, Gautreau A, Lamarine M, Callebaut I, Thomas G, Goutebroze L (2001) Normal membrane localization and actin association of the NF2 tumor suppressor protein are dependent on folding of its N-terminal domain. J Cell Sci 114:1901–1912.
11. James MF, Manchanda N, Gonzalez-Agosti C, Hartwig JH, Ramesh V (2001) The neurofibromatosis 2 protein product merlin selectively binds F-actin but not G-actin, and stabilizes the filaments through a lateral association. Biochem J 356:377–386.
12. Xu HM, Gutmann DH (1998) Merlin differentially associates with the microtubule and actin cytoskeleton. J Neurosci Res 51:403–415.
13. Bretscher A, Edwards K, Fehon RG (2002) ERM proteins and merlin: integrators at the cell cortex. Nat Rev Mol Cell Biol 3:586–599.
14. Curto M, McClatchey AI (2008) Nf2/Merlin: a coordinator of receptor signalling and intercellular contact. Br J Cancer 98:256–262.
15. Pearson MA, Reczek D, Bretscher A, Karplus PA (2000) Structure of the ERM protein moesin reveals the FERM domain fold masked by an extended actin binding tail domain. Cell 101:259–270.
16. Smith WJ, Nassar N, Bretscher A, Cerione RA, Karplus PA (2003) Structure of the active N-terminal domain of Ezrin. Conformational and mobility changes identify keystone interactions. J Biol Chem 278:4949–4956.
17. Kang BS, Cooper DR, Devedjiev Y, Derewenda U, Derewenda ZS (2002) The structure of the FERM domain of merlin, the neurofibromatosis type 2 gene product. Acta Crystallogr D Biol Crystallogr 58:381–391.
18. Shimizu T, Seto A, Maita N, Hamada K, Tsukita S, Hakoshima T (2002) Structural basis for neurofibromatosis type 2. Crystal structure of the merlin FERM domain. J Biol Chem 277:10332–10336.
19. Edwards SD, Keep NH (2001) The 2.7 A crystal structure of the activated FERM domain of moesin: an analysis of structural changes on activation. Biochemistry 40:7061–7068.
20. Matsui T, Maeda M, Doi Y, Yonemura S, Amano M, Kaibuchi K, Tsukita S (1998) Rho-kinase phosphorylates COOH-terminal threonines of ezrin/radixin/moesin (ERM) proteins and regulates their head-to-tail association. J Cell Biol 140:647–657.
21. Shaw RJ, Paez JG, Curto M, Yaktine A, Pruitt WM, Saotome I, O'Bryan JP, Gupta V, Ratner N, Der CJ, Jacks T, McClatchey AI (2001) The Nf2 tumor suppressor, merlin, functions in Rac-dependent signaling. Dev Cell 1:63–72.
22. Hamada K, Shimizu T, Yonemura S, Tsukita S, Hakoshima T (2003) Structural basis of adhesion-molecule recognition by ERM proteins revealed by the crystal structure of the radixin-ICAM-2 complex. EMBO J 22:502–514.
23. Terawaki S, Maesaki R, Okada K, Hakoshima T (2003) Crystallographic characterization of the radixin FERM domain bound to the C-terminal region of the human Na+/H+-exchanger regulatory factor (NHERF). Acta Crystallogr D Biol Crystallogr 59:177–179.
24. Matsui T, Yonemura S, Tsukita S (1999) Activation of ERM proteins in vivo by Rho involves phosphatidylinositol 4-phosphate 5-kinase and not ROCK kinases. Curr Biol 9:1259–1262.
25. Fievet BT, Gautreau A, Roy C, Del Maestro L, Mangeat P, Louvard D, Arpin M (2004) Phosphoinositide binding and phosphorylation act sequentially in the activation mechanism of ezrin. J Cell Biol 164:653–659.
26. Laulajainen M, Muranen T, Carpen O, Gronholm M (2008) Protein kinase A-mediated phosphorylation of the NF2 tumor suppressor protein merlin at serine 10 affects the actin cytoskeleton. Oncogene 27:3233–3243.
27. Rong R, Surace EI, Haipek CA, Gutmann DH, Ye K (2004) Serine 518 phosphorylation modulates merlin intramolecular association and binding to critical effectors important for NF2 growth suppression. Oncogene 23:8447–8454.
28. Alfthan K, Heiska L, Gronholm M, Renkema GH, Carpen O (2004) Cyclic AMP-dependent protein kinase phosphorylates merlin at serine 518 independently of p21-activated kinase and promotes merlin-ezrin heterodimerization. J Biol Chem 279:18559–18566.
29. Nguyen R, Reczek D, Bretscher A (2001) Hierarchy of merlin and ezrin N- and C-terminal domain interactions in homo- and heterotypic associations and their relationship to binding of scaffolding proteins EBP50 and E3KARP. J Biol Chem 276:7621–7629.
30. Murthy A, Gonzalez-Agosti C, Cordero E, Pinney D, Candia C, Solomon F, Gusella J, Ramesh V (1998) NHE-RF, a regulatory cofactor for Na(+)-H+ exchange, is a common interactor for merlin and ERM (MERM) proteins. J Biol Chem 273:1273–1276.
31. Morrison H, Sherman LS, Legg J, Banine F, Isacke C, Haipek CA, Gutmann DH, Ponta H, Herrlich P (2001) The NF2 tumor suppressor gene product, merlin, mediates contact inhibition of growth through interactions with CD44. Genes Dev 15:968–980.
32. Hamada K, Shimizu T, Matsui T, Tsukita S, Hakoshima T (2000) Structural basis of the membrane-targeting and unmasking mechanisms of the radixin FERM domain. EMBO J 19:4449–4462.
33. Li Q, Nance MR, Kulikauskas R, Nyberg K, Fehon R, Karplus PA, Bretscher A, Tesmer JJ (2007) Self-masking in an intact ERM-merlin protein: an active role for the central alpha-helical domain. J Mol Biol 365: 1446–1459.
34. Scoles DR, Huynh DP, Morcos PA, Coulsell ER, Robinson NG, Tamanoi F, Pulst SM (1998) Neurofibromatosis 2 tumour suppressor schwannomin interacts with betaII-spectrin. Nat Genet 18:354–359.
35. Gutmann DH, Geist RT, Xu H, Kim JS, Saporito-Irwin S (1998) Defects in neurofibromatosis 2 protein function can arise at multiple levels. Hum Mol Genet 7: 335–345.
36. Stokowski RP, Cox DR (2000) Functional analysis of the neurofibromatosis type 2 protein by means of disease-causing point mutations. Am J Hum Genet 66: 873–891.
37. Lawrence MC, Colman PM (1993) Shape complementarity at protein/protein interfaces. J Mol Biol 234:946–950.
38. Lallemand D, Saint-Amaux AL, Giovannini M (2009) Tumor-suppression functions of merlin are independent of its role as an organizer of the actin cytoskeleton in Schwann cells. J Cell Sci 122:4141–4149.
39. LaJeunesse DR, McCartney BM, Fehon RG (1998) Structural analysis of Drosophila merlin reveals functional domains important for growth control and subcellular localization. J Cell Biol 141:1589–1599.
40. Kitano K, Yusa F, Hakoshima T (2006) Structure of dimerized radixin FERM domain suggests a novel masking motif in C-terminal residues 295–304. Acta

Crystallogr Sect F Struct Biol Cryst Commun 62: 340–345.
41. Henrick K, Thornton JM (1998) PQS: a protein quaternary structure file server. Trends Biochem Sci 23: 358–361.
42. Janin J, Rodier F (1995) Protein-protein interaction at crystal contacts. Proteins 23:580–587.
43. Vonrhein C, Flensburg C, Keller P, Sharff A, Smart O, Paciorek W, Womack T, Bricogne G (2011) Data processing and analysis with teh autoPROC toolbox. Acta Crystallogr D Biol Crystallogr 67:293–302.
44. Kabsch W (2010) XDS. Acta Crystallogr D Biol Crystallogr 66:125–132.
45. Evans P (2006) Scaling and assessment of data quality. Acta Crystallogr D Biol Crystallogr 62:72–82.
46. McCoy AJ, Grosse-Kunstleve RW, Adams PD, Winn MD, Storoni LC, Read RJ (2007) Phaser crystallographic software. J Appl Crystallogr 40:658–674.
47. Collaborative Computational Project N (1994) The CCP4 Suite: programs for protein crytsallography. Acta Crystallogr D Biol Crystallogr D50:760–763.
48. Bricogne G, Blanc E, Brandl M, Flensburg C, Keller P, Paciorek P, Roversi P, Sharff A, Smart O, Vonrhein C, Womack T (2010) BUSTER version 2.9. Cambridge, United Kingdom: Global Phasing Ltd.
49. Emsley P, Cowtan K (2004) Coot: model-building tools for molecular graphics. Acta Crystallogr D Biol Crystallogr 60:2126–2132.
50. Smart OS, Brandl M, Flensburg C, Keller P, Paciorek W, Vonrhein C, Womack TO, Bricogne G (2008) Refinement with local structure similarity restraints (LSSR) enables exploitation of information from related structures and facilitates use of NCS. Abstr Annu Meet Am Crystallogr Assoc, Knoxville, TN. abstr. TP139.

SUPPLEMENTARY INFORMATION

Unfurling of the band 4.1, ezrin, radixin, moesin (FERM) domain of the merlin tumor suppressor

S.D. Yogesha,[1] Andrew J. Sharff,[2] Marco Giovannini,[3] Gerard Bricogne,[2] and Tina Izard[1*]

Supplementary Materials and Methods

Liquid chromatography/mass spectrometry analyses of merlin head:tail crystals

Merlin head:tail crystals were washed twice in reservoir solution (0.2 M ammonium sulfate and 5% PEG 4000) and then dissolved in 10 mM Tris (pH 8). The dissolved crystals were treated with 0.5 mM DTT for 1 hr at 37 ºC, followed by treatment with 2 mM iodoacetamide for 1 hr at ambient temperature, to reduce and carbamidomethylate cysteine residues. The protein was subjected to proteolysis with trypsin (35 ng) and the resulting merlin peptides were analyzed by liquid chromatography coupled with tandem mass spectrometry (LC-MS/MS) by our in-house proteomics core. The resulting peptides were first loaded onto a 360 × 100 μm fused silica capillary (PolyMicro Technologies, Phoenix, AZ) pre-column packed with 3 cm of C12 packing material (Jupiter Proteo C12, 4 μm particle size). Salts were removed by washing with 0.1 M acetic acid in 1% acetonitrile and the column was placed in line with a 360 × 100 μm fused silica capillary column packed with 20 cm of C12 material. The peptides were eluted with a gradient consisting of 5% to 55% acetonitrile in 50 min, using a 1,100 series HPLC pump (Agilent Technologies, Santa Clara, CA). A flow rate of 200 nl/min was achieved at the reverse phase column by splitting the flow delivered from the HPLC. Peptides were gradient-eluted and ionized (1.7 kV) by placing a nano-electrospray ionization source (Triversa Nanomate, Advion, Ithaca, NY) into an LTQ-Orbitrap mass spectrometer (Thermo Scientific, San Jose, CA). The LTQ-Orbitrap instrument was operated in a data-dependent mode with dynamic exclusion enabled. The data-dependent method consisted of acquisition of a full scan mass spectrum (m/z 350 – 2000) using the Orbitrap as the analyzer, followed by ten tandem mass spectra (MS/MS) of the ten most abundant ions in the initial full scan. Precursor ions selected for MS/MS were fragmented by collision-activated dissociation (CAD), and the MS/MS scans were acquired using the ion trap as the analyzer. Data were processed using a raw file processing pipeline that extracts tandem mass spectra from the raw data files, which filters the data for spectral quality using the SPEQUAL algorithm,[1] and concatenates the high-quality spectra for database searching via a clustered version of Mascot.[2] Searches were performed against the IPI human protein database. Mascot search results were loaded into Scaffold (Proteome Software, Portland, OR) for statistical analysis followed by manual verification of all peptide assignments. All of the merlin peptides detected are presented in the Supplementary Table.

SUPPLEMENTARY INFORMATION

Supplementary Figure Legends

Supplementary Figure S1. Unfurling of the merlin F2 domain. The F1 subdomain (residues 20-82 and 91-100) is shown in yellow, the F2 subdomain (residues 101-158 and 178-215) is shown in green, and the F3 motif (residues 216-313) is shown in magenta.

(A) Zoomed-in stereo view of the final $2F_o$-F_c electron density map of the F2 α3-α4 loop region. The contour level of the electron density map is 1σ and the resolution is 2.64 Å. Water molecules are shown as a red sphere. Oxygen atoms are in red, nitrogen in blue and carbon in yellow, green, or magenta for the F1-F3 subdomain, respectively. Some residues are labeled.

(B) Zoomed-out view of the merlin dimer looking down the dyad in the same orientation as in panel (A). Some secondary structure elements are labeled with the extension 'b' indicating its location on the F2 subdomain. Residues from the F2 α3-α4 loop are shown in ball-and-stick representation with the remainder of the molecule as a cartoon. The black square indicates the region that is shown in panel (A).

Supplementary Figure S2. Unfurling of the merlin F2 subdomain is likely triggered by the tail domain.

(A) Superposition our 2.64 Å unfurled merlin FERM domain (yellow, green, and magenta) onto the 3 Å full-length moesin crystal structure (white, black, and red; PDB entry 2i1k) and the 2.1 Å truncated moesin crystal structure (grey; PDB entry 2i1j). In the full-length moesin structure, the *C*-terminus (indicated by an arrow that points at moesin residue 320) of the moesin 'A' α-helix (labeled, shown in black, residues 299-320) would have to shift to allow the unfurling of its F2 subdomain.

(B) Superposition of our unfurled merlin structure (orange) onto the moesin head:tail structure (white and black) and the closed, unbound merlin head structure (PDB entry 1h4r; cyan). Both molecules in the asymmetric unit are shown for the moesin head:tail complex and for the closed, unbound merlin FERM structures. The former are very similar with *r.m.s.d.* of 0.14 Å for 2,174 atoms. While the loop succeeding β-strand β6c in our unfurled merlin structure resembles that of the closed moesin head:tail structure (indicated by one arrow on the right), there is further movement in the α-helix α3b and its following loop (indicated by two arrows on the left) in the moesin head:tail structure (green) when compared to the closed, unbound merlin head structure (cyan).

SUPPLEMENTARY INFORMATION

Supplementary Figure S3. Sequence alignment of the FERM domains of moesin versus merlin.

Residues that are identical in the two structures are indicated by an asterisk in the moesin (Moe) sequence (top sequence). The F1, F2, and F3 subdomains are indicated. The four α-helices are highlighted in red (moesin residues 95-112, merlin residues 112-128), yellow (moesin residues 118-135, merlin residues 135-150), green (moesin residues 164-179, merlin residues 181-196), and blue (moesin residues 183-196, merlin residues 202-213), respectively. The α-helix α2b is disordered in our unfurled structure of the merlin head domain. Underlined merlin residues (83-90 and 159-177) indicate disordered regions. A period above the moesin sequence indicates that this residue is involved in the moesin head:tail interface as seen in the crystal structure.[3] Italicized merlin residues in blue font indicate the region that unfurls, which is distinct from any FERM domain structure determined thus far. There are 22 identical residues in the merlin 150-201 region while there are 27 and 38 identical residues in the merlin 98-149 and 202-253 regions, respectively.

REFERENCES

1. Purvine S, Kolker N, Kolker E (2004) Spectral quality assessment for high-throughput tandem mass spectrometry proteomics. OMICS 8:255-265.
2. Perkins DN, Pappin DJ, Creasy DM, Cottrell JS (1999) Probability-based protein identification by searching sequence databases using mass spectrometry data. Electrophoresis 20:3551-3567.
3. Pearson MA, Reczek D, Bretscher A, Karplus PA (2000) Structure of the ERM protein moesin reveals the FERM domain fold masked by an extended actin binding tail domain. Cell 101:259-270.

Supplementary Figure S1

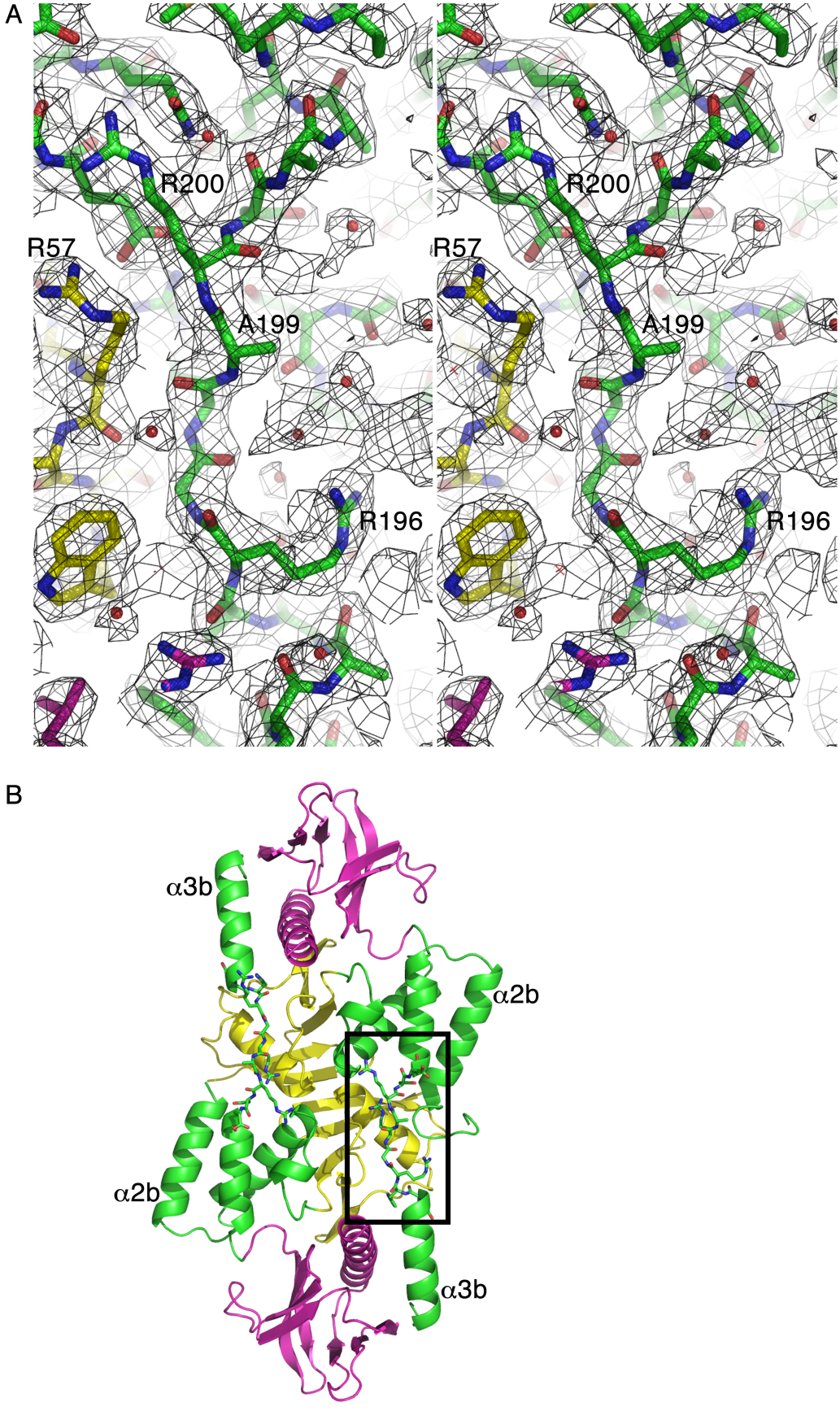

Supplementary Figure S2

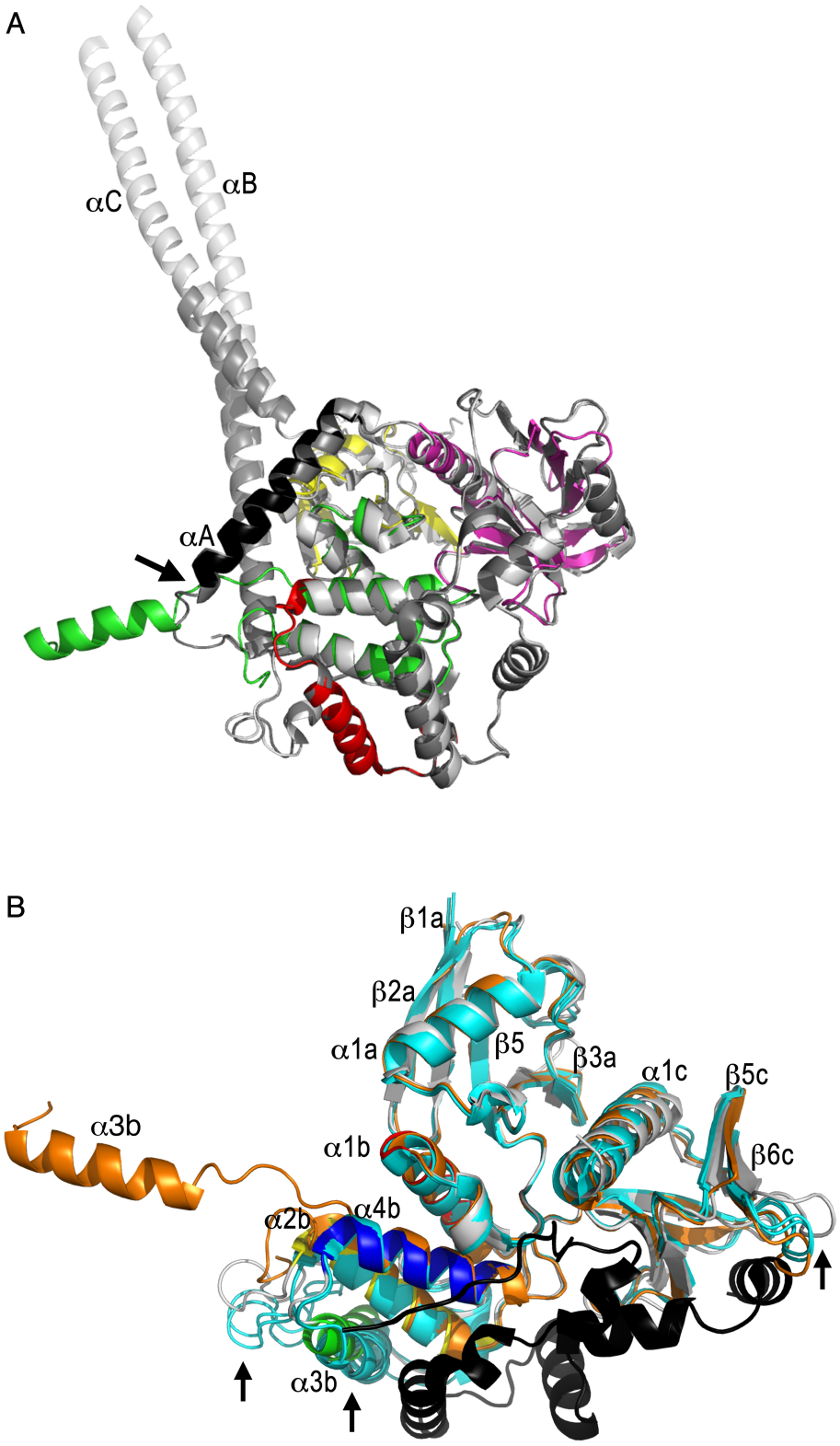

Supplementary Figure S3

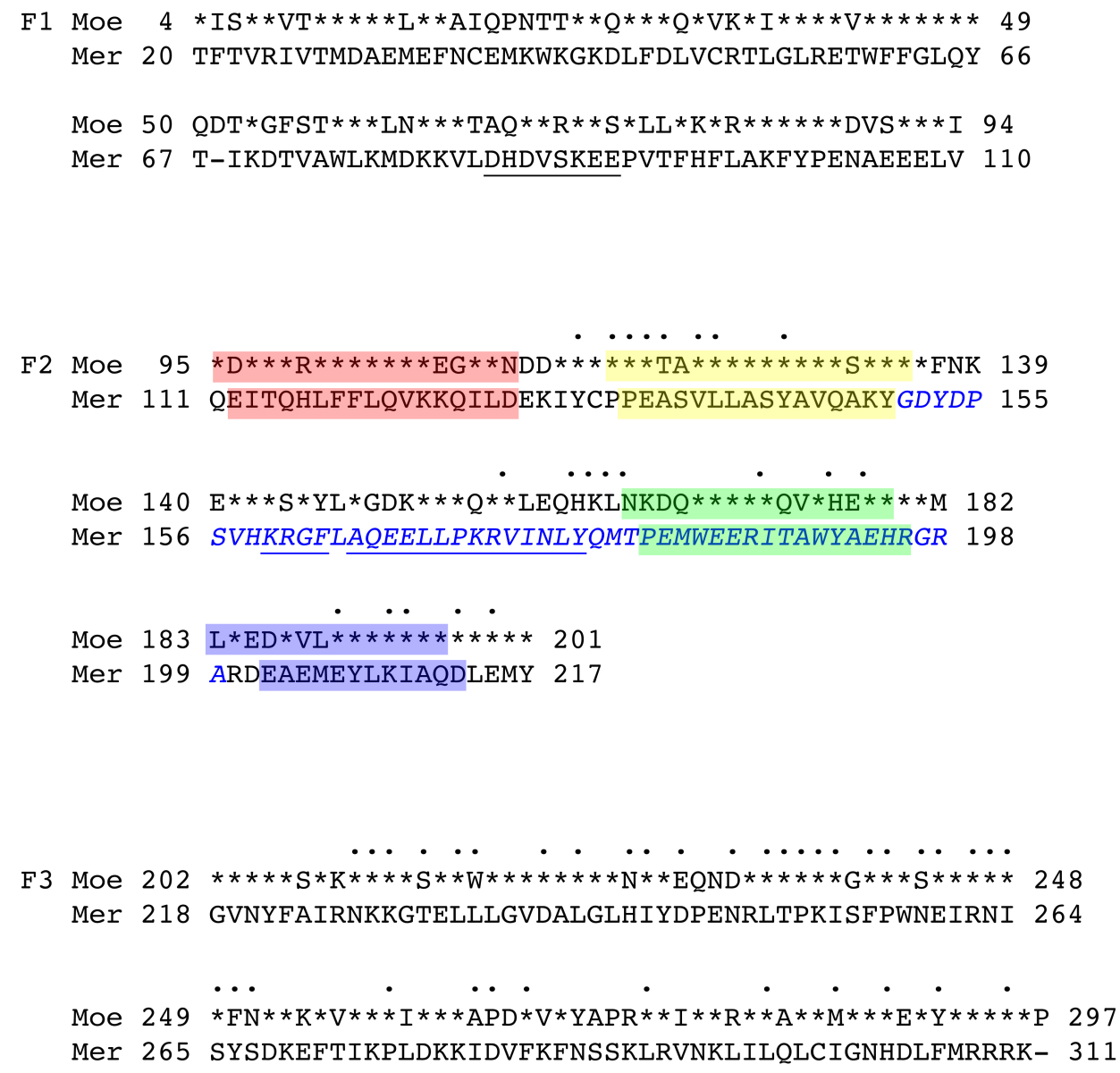

Supplementary Table. Peptides identified from MS/MS. Peptides identified in the mass spectrometric experiment are listed. Amino acids listed as lower case letters indicate that this amino acid is modified: c, carbamidomethylated cysteine and m, oxidized methionine. For simplicity only one peptide was listed for each possible modification since the masses identified are the same. Theoretical masses were calculated and compared to observed masses to determine part per million errors. The table lists all observed masses for each peptide. Note that peptides were identified for both the head and the tail domain of our crystals and thus confirming that our crystals contain both domains, in particular the tail domain, which is disordered in our structure.

		Theoretical (monoisotropic)				Observed (monoisotropic)				Error calculations (PPM)			
Peptide sequence	Residues	MH+1	MH+2	MH+3	MH+4	MH+1	MH+2	MH+3	MH+4	+1	+2	+3	+4
IVTMDAEMEFNcEMK	26-40	1847.7682	924.3878	616.5943	462.6975		924.3881	616.5937			0.32	-0.97	
IVTMDAEMEFNcEmK	26-40	1863.7632	932.3852	621.9259	466.6962		932.3848	621.925			-0.43	-1.45	
IVTmDAEMEFNcEmK	26-40	1879.7581	940.3827	627.2575	470.695		940.3805	627.2562			-2.34	-2.07	
IVTMDAEMEFNcEmKWK	26-42	2177.9374	1089.472	726.6507	545.2398		1089.474	726.6511			1.56	0.55	
IVTmDAEMEFNcEmKWK	26-42	2193.9323	1097.47	731.9823	549.2385		1097.47	731.9813			-0.09	-1.37	
IVTmDAEmEFNcEmK	26-40	1895.753	948.3801	632.5892	474.6937		948.3798	632.5884			-0.32	-1.26	
GKDLFDLVcR	43-52	1222.6249	611.8161	408.2161	306.4117	1222.624	611.8145			-0.41	-2.62		
DLFDLVcR	45-52	1037.5084	519.2579	346.5077		1037.508	519.2554			0.00	-4.81		
KVLDHDVSKEEPVTFHFLAK	80-99	2339.2394	1170.123	780.418	585.5653			780.418	585.5646			0.00	-1.20
VLDHDVSK	81-88	912.4785	456.7429	304.831		912.4783	456.7418	304.8305		-0.22	-2.41	-1.64	
VLDHDVSKEEPVTFHFLAK	81-99	2211.1444	1106.076	737.7197	553.5416		1106.074	737.7186	553.5414		-1.72	-1.49	-0.36
EEPVTFHFLAK	89-99	1317.6838	659.3455	439.8994	330.1764	1317.684	659.3446	439.8979		0.15	-1.36	-3.41	
FYPENAEEELVQEITQHLFFLQVK	100-123	2951.4826	1476.245	984.499	738.6261		1476.242	984.4991	738.6259		-2.10	0.10	-0.27
KQILDEK	124-130	873.504	437.2556			873.5035	437.2545			-0.57	-2.52		
QILDEK	125-130	745.409	373.2082			745.408	373.2071			-1.34	-2.95		
IYcPPEASVLLASYAVQAK	131-149	2080.0783	1040.543	694.031	520.775		1040.54	694.0291			-3.08	-2.74	
YGDYDPSVHK	150-159	1180.5269	590.7671	394.1805		1180.526	590.7658	394.1789		-0.42	-2.20	-4.06	
YGDYDPSVHKR	150-160	1336.628	668.8177	446.2142	334.9125	1336.626	668.8159	446.2123	334.9117	-1.27	-2.69	-4.26	-2.39
GFLAQEELLPK	161-171	1244.6885	622.8479	415.5677	311.9276	1244.688	622.8467	415.5675		-0.08	-1.93	-0.48	
GFLAQEELLPKR	161-172	1400.7896	700.8985	467.6014	350.9529		700.8981	467.6003			-0.57	-2.35	
RVINLYQMTPEMWEER	172-187	2095.0099	1048.009	699.0082	524.5079		1048.01	699.0079	524.5071		1.43	-0.43	-1.53
RVINLYQMTPEmWEER	172-187	2111.0049	1056.006	704.3398	528.5067		1056.007	704.3386			0.38	-1.70	
RVINLYQmTPEmWEER	172-187	2126.9998	1064.004	709.6714	532.5054		1064.004	709.6699			0.28	-2.11	
VINLYQMTPEMWEER	173-187	1938.9088	969.9581	646.9745	485.4827		969.9578	646.9737			-0.31	-1.24	
VINLYQMTPEmWEER	173-187	1954.9037	977.9555	652.3061	489.4814		977.9514	652.304			-4.19	-3.22	

VINLYQmTPEmWEER	173-187	1970.8987	985.953	657.6377	493.4801		985.9514	657.6366			-1.62	-1.67	
ITAWYAEHR	188-196	1146.5691	573.7882	382.8612		1146.567	573.7858	382.8591		-1.92	-4.18	-5.49	
ARDEAEMEYLK	199-209	1354.6307	677.819	452.2151	339.4131		677.8171	452.213			-2.80	-4.64	
ARDEAEmEYLK	199-209	1370.6257	685.8165	457.5467	343.4119	1370.623	685.8146	457.5447		-1.75	-2.77	-4.37	
DEAEMEYLK	201-209	1127.4925	564.2499	376.5024		1127.493	564.2488			0.35	-1.95		
DEAEmEYLK	201-209	1143.4874	572.2474	381.834		1143.488	572.2466			0.52	-1.40		
IAQDLEMYGVNYFAIR	210-225	1902.9418	951.9746	634.9855	476.4909		951.9744	634.985			-0.21	-0.79	
IAQDLEmYGVNYFAIR	210-225	1918.9368	959.972	640.3171	480.4896		959.9689	640.3151			-3.23	-3.12	
KGTELLLGVDALGLHIYDPENR	228-249	2423.2929	1212.15	808.4358	606.5787		1212.151	808.4365	606.5786		0.66	0.87	-0.16
GTELLLGVDALGLHIYDPENR	229-249	2295.1979	1148.103	765.7375	574.5549		1148.104	765.7373	574.5546		0.78	-0.26	-0.52
ISFPWNEIR	254-262	1161.6051	581.3062	387.8732		1161.606	581.3057			0.60	-0.86		
NISYSDKEFTIKPLDK	263-278	1897.9906	949.4989	633.335	475.2531		949.4984	633.34	475.2523		-0.53	7.89	-1.68
EFTIKPLDK	270-278	1090.6143	545.8108	364.2096		1090.617	545.8099	364.2089		2.29	-1.65	-1.92	
EFTIKPLDKK	270-279	1218.7093	609.8583	406.9079	305.4328	1218.707	609.8571	406.9068	305.4322	-1.72	-1.97	-2.70	-1.96
KIDVFK	279-284	749.4556	375.2314			749.455	375.2308			-0.80	-1.60		
IDVFKFNSSK	280-289	1184.631	592.8191	395.5485			592.8181	395.548		-1.69	-1.26		
LILQLcIGNHDLFmR	295-309	1858.9666	929.9869	620.3271	465.4971		929.9875	620.327			0.65	-0.16	
LSmEIEKEK	517-525	1122.5711	561.7892	374.8619			561.7877	374.8612			-2.67	-1.87	
LSmEIEK	517-523	865.4335	433.2204				433.2195				-2.08		
SKHLQEQLNELKTEIEALK	532-550	2251.2292	1126.118	751.0813	563.5628			751.0811	563.5618			-0.27	-1.77
HLQEQLNELKTEIEALK	534-550	2036.1022	1018.555	679.3723	509.781		1018.556	679.3724	509.7802		0.69	0.15	-1.57
TEIEALK	544-550	803.4509	402.2291			803.4506	402.2284			-0.37	-1.74		
ERETALDILHNENSDR	553-568	1911.9155	956.4614	637.9767	478.7343			637.9765	478.7336			-0.31	-1.46
ETALDILHNENSDR	555-568	1626.7718	813.8895	542.9288	407.4484		813.8898	542.928			0.37	-1.47	
VAFFEEL	589-595	854.4294	427.7184			854.4294				0.00			
Peptide sequence	Residues	MH+1	MH+2	MH+3	MH+4	MH+1	MH+2	MH+3	MH+4	+1	+2	+3	+4
		Theoretical (monoisotropic)				Observed (monoisotropic)				Error calculations (PPM)			